DOI: 10.1002/ejic.200700419

Aqueous Reduction of $[Cp^*_2W_2O_5]$: Characterization of the Triangular Clusters $[Cp^*_3W_3O_4(OH)_2]^{2+}$ and $[Cp^*_3W_3O_6]^+$ – Comparison with Molybdenum

Chiara Dinoi,[a] Pelin Sözen,[b] Gülnur Taban,[b] Deniz Demir,[b] Funda Demirhan,*[b] Petr Prikhodchenko,[c] Jenny Gun,[c] Ovadia Lev,[c] Jean-Claude Daran,[a] and Rinaldo Poli*[a]

Keywords: Tungsten / O ligands / Metal clusters / Density functional calculations

Zinc reduction of $Cp^*_2W_2O_5$ in an acidified water–methanol medium affords the green 3-electron trinuclear cluster $[Cp^*_3W_3O_4(OH)_2]^{2+}$, isolated and crystallographically characterized as the triflate salt, **1**. Upon exposure to air, this complex is oxidized to a related 2-electron cluster, $[Cp^*_3W_3O_6]^+$, which was crystallized and characterized in three different salts, **2**–**4**. The 3-electron cluster exhibits a near-tetragonal frozen-glass EPR spectrum, and it shows evidence of coupling of the unpaired electron to only one of the three W atoms. The two-electron cluster is diamagnetic. An electrospray ionization MS^n study revealed a stepwise expulsion of neutral $[Cp^*WO_2]$ units as the main fragmentation process. DFT calculations unveiled the intimate details of the electronic structures of these complexes and fully rationalized the structural and spectroscopic properties.

Introduction

Aqueous organometallic chemistry is attracting growing interest because of its "green" impact[1–3] and because of its potential in catalytic[4,5] and biomedical applications.[6] Although this area is widely explored for low-valent systems, usually upon appending hydrophilic functionalities to the ligand periphery to increase solubility in an aqueous environment,[7–9] studies of high-oxidation organometallics are still rather scarce.[10–12] For redox-active metals, these studies are particularly interesting, as they may open the way to electrocatalytic applications.[12]

In a recent contribution,[13] we reported that the zinc reduction of $Cp^*_2Mo_2O_5$ in a strongly acidic (CF_3COOH or CF_3SO_3H) mixed H_2O/MeOH medium affords the trinuclear mixed-valence (Mo_3^{13+}) cluster $[Cp^*_3Mo_3O_2(OH)_4]^{2+}$. The ion adopts a nearly equilateral triangular shape; each edge is bridged by two ligands. The distortion of the triangle is caused by one edge that is bridged by two OH groups, whereas the other two edges are bridged by one O atom and one OH group. As a consequence, the former edge is slightly longer than the latter ones. Although the number of bridging OH versus O groups was not revealed directly by the X-ray structural analysis, it was suggested indirectly by the same technique through the existence of short hydrogen-bonding contacts (or lack thereof) between the Mo_3O_6 core and the two CF_3CO_2 and CF_3SO_3 anions, and this was confirmed by comparison with a DFT geometry-optimized model, by EPR spectrometry, and by magnetic susceptibility measurements.

In this contribution, we examine the parallel behavior of the pentamethylcyclopentadienyltungsten system and report the isolation and characterization of two new redox-related tritungsten oxido clusters, $[Cp^*_3W_3O_6]^+$ and $[Cp^*_3W_3O_4(OH)_2]^{2+}$.

[a] Laboratoire de Chimie de Coordination, UPR CNRS 8241 liée par convention à l'Université Paul Sabatier et à l'Institut National Polytechnique de Toulouse,
205 Route de Narbonne, 31077 Toulouse Cedex, France
Fax: +33-561553003
E-mail: Rinaldo.Poli@lcc-toulouse.fr
[b] Celal Bayar University, Faculty of Sciences & Liberal Arts, Department of Chemistry,
45030 Muradiye-Manisa, Turkey
[c] Laboratory of Environmental Chemistry, The Casali Institute of Applied Chemistry, The Hebrew University of Jerusalem,
Jerusalem 91904, Israel

Supporting information for this article is available on the WWW under http://www.eurjic.org or from the author.

Results and Discussion

The $[Cp^*_3W_3O_4(OH)_2]^{2+}$ Cluster

The reduction of $[Cp^*_2W_2O_5]$ was carried out under the same conditions previously used for the reduction of $[Cp^*_2Mo_2O_5]$, namely by metallic zinc in an acidic H_2O/MeOH mixed solvent. MeOH is necessary to increase the solubility of the starting material. The reaction was carried out in the presence of two different acids, trifluoroacetic acid and trifluoromethylsulfonic (triflic) acid. As for the

Mo analogue, a series of color changes was observed over a period of three days, yielding a final green solution through an intermediate orange-red color. Crystallization of the final green product was successful in the case of the triflic acid reaction, revealing the nature of the compound as $[Cp^*_3W_3O_4(OH)_2](CF_3SO_3)_2{\cdot}2H_2O$ (**1**). Thus, the reaction stoichiometry is as shown in Equation (1). The oxidation state of tungsten in the final product is +5, yielding a 3-electron W_3^{15+} cluster. Compound **1** is quite soluble in CH_2Cl_2 and its solutions are air sensitive, and they turn rapidly to orange when exposed to the atmosphere. The nature of the orange product is shown in the next section.

$$3[Cp^*_2W_2O_5] + 3Zn + 10H^+ \rightarrow 2[Cp^*_3W_3O_4(OH)_2]^{2+} + 3H_2O + 3Zn^{2+} \quad (1)$$

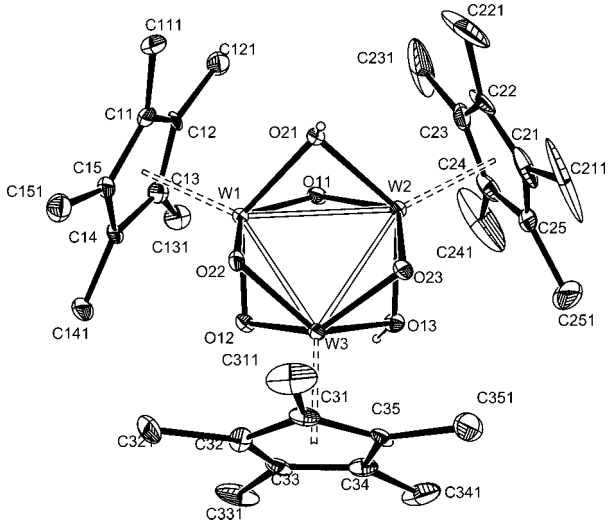

Figure 1. An ORTEP view of the dication in compound $[Cp^*_3W_3O_4(OH)_2](CF_3SO_3)_2{\cdot}2H_2O$ (**1**).

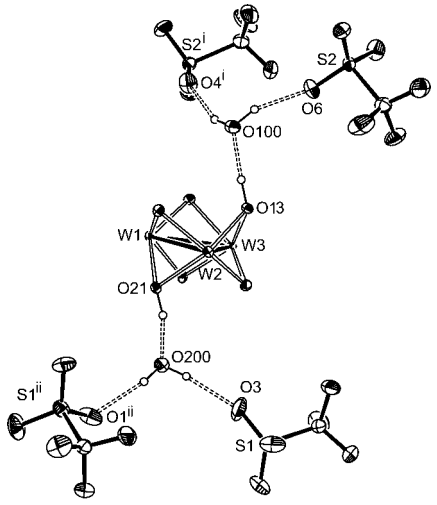

Figure 2. An ORTEP view of compound **1** that highlights the H-bonding interactions between dication, anions, and interstitial water molecules. The Cp* ligands bonded to the W_3 cluster are omitted for clarity [symmetry codes: (i) 3/2 – *x*, *y* – 1/2, 1 – *z*; (ii) 1/2 – *x*, *y* – 1/2, –*z*].

Table 1. Selected bond lengths and angles for the trinuclear clusters in all compounds.[a]

Bond lengths [Å]				
	1	**2**[b]	**3**	**4**
W1–W2	2.7416(3)	2.6565(4)	2.6685(5)	2.6637(8)
W1–W3	2.6545(3)	2.6505(5)	2.6657(5)	2.6614(9)
W2–W3	2.7485(3)		2.6849(5)	2.6606(8)
W1–O11	1.882(4)	1.958(5)	1.980(6)	1.917(8)
W1–O12	1.905(4)	1.975(4)	1.967(6)	1.931(8)
W1–O21	2.076(3)	1.967(4)	1.949(6)	1.958(8)
W1–O22	2.009(3)	1.952(4)	1.955(5)	1.973(8)
W1–CG1	2.034(2)	2.0507(3)	2.054(4)	2.0555(6)
W2–O11	1.979(4)	1.948(5)	1.937(6)	1.935(8)
W2–O13	2.038(4)		1.968(5)	1.944(8)
W2–O21	2.045(3)	1.960(4)	1.954(5)	1.966(8)
W2–O23	2.001(4)		1.977(5)	1.967(8)
W2–CG2	2.003(2)	2.0400(4)	2.068(7)	2.0549(6)
W3–O12	2.003(4)		1.960(6)	1.955(8)
W3–O13	2.080(4)		1.998(5)	1.936(8)
W3–O23	1.872(3)		1.962(6)	1.945(8)
W3–O22	1.899(3)		1.963(6)	1.952(8)
W3–CG3	2.050(2)		2.053(8)	2.0510(6)
Bond angles [°]				
W2–W1–W3	61.216(8)	60.075(7)	60.443(14)	59.95(2)
W1–W3–W2	60.955(7)		59.828(13)	60.07(2)
W1–W2–W3	57.829(7)	59.843(7)	59.728(13)	59.98(2)
CG1–W1–O11	111.29(11)	113.53(13)	113.2(3)	112.5(2)
CG1–W1–O12	112.01(11)	113.00(13)	112.7(3)	110.3(2)
CG1–W1–O21	114.19(10)	112.67(13)	113.6(3)	115.7(2)
CG1–W1–O22	113.22(10)	112.96(13)	113.2(3)	114.0(2)
O11–W1–O12	93.18(15)	84.6(2)	85.1(2)	87.2(3)
O11–W1–O22	134.61(16)	134.02(18)	133.6(2)	133.4(3)
O12–W1–O22	78.29(14)	76.75(19)	76.8(2)	74.9(3)
O11–W1–O21	73.59(14)	77.6(2)	75.7(2)	76.5(3)
O12–W1–O21	133.66(15)	133.80(19)	133.6(2)	134.0(3)
O22–W1–O21	80.67(14)	85.72(19)	86.6(2)	85.8(3)
CG2–W2–O11	114.72(10)	113.40(14)	112.0(3)	114.0(2)
CG2–W2–O23	113.47(10)		114.0(3)	113.2(2)
CG2–W2–O13	114.14(10)	112.61(13)	111.5(2)	112.9(2)
CG2–W2–O21	115.30(10)		114.1(2)	113.9(2)
O11–W2–O23	131.80(14)	85.23(19)	133.9(2)	132.8(3)
O11–W2–O13	87.65(15)		86.2(2)	87.0(3)
O23–W2–O13	72.14(14)	77.16(19)	76.0(2)	75.4(3)
O11–W2–O21	72.32(15)		76.6(2)	75.9(3)
O23–W2–O21	88.19(14)		86.2(2)	84.9(3)
O13–W2–O21	130.57(14)	133.2(3)	134.4(2)	133.2(3)
CG3–W3–O23	111.55(11)		114.9(3)	114.5(2)
CG3–W3–O22	112.91(10)		112.07(18)	113.7(2)
CG3–W3–O12	112.40(10)		111.4(3)	111.6(2)
CG3–W3–O13	113.53(10)		114.06(18)	111.5(2)
O23–W3–O22	93.60(15)		86.4(2)	86.6(3)
O23–W3–O12	134.86(15)	134.8(3)	133.7(2)	133.9(3)
O22–W3–O12	78.58(15)		75.6(2)	75.0(3)
O23–W3–O13	73.76(15)		76.8(2)	75.9(3)
O22–W3–O13	133.32(15)		133.7(2)	134.8(3)
O12–W3–O13	79.89(15)		85.6(2)	87.7(3)
W1–O11–W2	90.44(15)	85.70(18)	86.3(2)	87.5(3)
W1–O12–W3	85.55(14)	85.12(17)	85.9(2)	86.5(3)
W2–O13–W3	83.74(13)	84.91(17)	85.8(2)	86.6(3)
W2–O21–W1	83.39(13)		85.5(2)	85.5(3)
W3–O22–W1	85.53(14)		85.9(2)	85.6(3)
W3–O23–W2	90.36(15)		85.2(2)	85.5(3)

[a] CGn is the center of gravity of the Cp* ligand bonded to atom Wn. [b] This structure has a symmetry imposed C_2 axis passing through atoms W2 and the midpoint of the W1–W1^i bond. Numbering scheme correspondence: W3=W1^i; O12 = O22^i; symmetry code: (i) –*x*, *y*, –*z* + 3/2.

The structure of the dication is shown in Figure 1, whereas Figure 2 illustrates the arrangement of the anions and the interstitial H_2O molecules relative to the trimetallic cluster. Relevant bonding parameters are collected in Table 1. The H atoms on the bridging OH groups could not be directly located from the diffraction data, but their presence is clearly demonstrated by the H-bonding network. Hydrogen bond contacts for compound **1** are available in the Supporting Information. As shown in Figure 2, the bridging atoms O13 and O21 establish short contacts with atoms O100 and O200 of the interstitial water molecules. The latter, in turn, establish short contacts with two different atoms of triflate anions: O100 with O6 but also with O4 of a second asymmetric unit; O200 with O3 but also with O1 of a third asymmetric unit. Close inspection of the difference Fourier map obtained after refinement of all heavy atoms revealed in fact the position of the H atoms on the interstitial H_2O molecules. This observation excludes the alternative formulation as a neutral $[Cp^*_3W_3O_6]$ complex with two interstitial CF_3SO_3H molecules, because in the latter case only one of the two H_2O protons would point towards an oxygen atom of the trifluoromethylsulfonate group, whereas the other one would point towards the bridging oxido group of the W_3 cluster. Although these considerations establish the presence of H atoms on O13 and O21, they provide no information on the absence or presence of H atoms on the other bridging O atoms, O11, O12, O22, and O23. This point will be addressed in further detail later by inspection of the spectroscopic properties and by comparison of the experimental (X-ray diffraction) and computed (DFT) bonding parameters.

A most informative structural feature is the variation of the W–W distances: the two bonds bridged by one O atom and one OH group, W1–W2 [2.7416(3) Å] and W2–W3 [2.7485(3) Å], are almost 0.1 Å longer than the bond bridged by two O groups, W1–W3 [2.6545(3) Å]. In addition, the W–OH distances [in the range 2.038–2.080 Å; average 2.06(2) Å] are statistically longer than the W–O distances [in the range 1.872–2.009 Å; average 1.94(6) Å]. Furthermore, the W–(μ–OH)–W angles [83.39(13) and 83.73(13)°] are smaller than the W–(μ-O)–W angles in the $W(\mu\text{-}O)_2W$ moiety [average 85.54(14)°]. The W–(μ-O)–W angles in the W(μ-O)(μ-OH)W moiety are even larger [average 90.40(15)°]. This is certainly a secondary effect related to the longer W–W distance.

The $[Cp^*_3W_3O_6]^+$ Cluster

The Triflate Structure – Compound 2

As stated above, exposure of solutions of compound **1** to air rapidly yields orange-red solutions. Crystallization from this oxidized solution yielded red crystals of compound **2**, which was shown by X-ray analysis to correspond to $[Cp^*_3W_3O_6](CF_3SO_3)$. This formulation is consistent with the spectroscopic properties and with a comparison between the experimental (X-ray diffraction) and computed (DFT) structural parameters, as shown in a later section. The cation is a mixed-valence $W_3^{V,V,VI}$ cluster, namely a 2-electron cluster. Thus, the transformation generating this cluster can be described as in Equation (2).

$$[Cp^*_3W_3O_4(OH)_2]^{2+} + [ox] \rightarrow [Cp^*_3W_3O_6]^+ + 2H^+ + [red] \quad (2)$$

Like compound **1**, compound **2** is soluble in CH_2Cl_2, but it is also fairly soluble in $MeOH/H_2O$ solvent mixtures. These solutions are relatively stable in air, but not indefinitely so, to ultimately yield colorless solutions, which apparently occurs faster at high pH values. ^1H NMR spectroscopic monitoring in $MeOD/D_2O$ reveals the formation of a single resonance (δ = 2.05 ppm) attributed to $[Cp^*WO_3]^-$[14] at neutral or basic pH, whereas several other products, yet to be identified, are obtained under strongly acidic conditions (pH 2: resonances at δ = 2.22, 2.19, 2.15).

The structure of **2** contains a simple anion and no interstitial solvent molecules, which firmly establishes the +1 charge of the cluster. However, the cation exhibits a symmetry-imposed disorder because of a twofold axis that

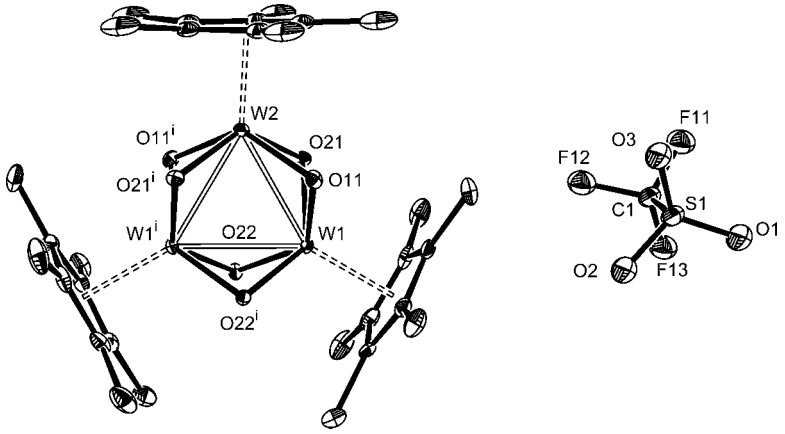

Figure 3. A view of the relative orientation of the cation and anion in the structure of $[Cp^*_3W_3O_6](CF_3SO_3)$ (**2**). Only one of the two symmetry-related orientations of the trifluoromethylsulfonate anion and of the Cp*(2) ligand are shown for the sake of clarity.

passes through atom W2 and through the midpoint of the W1–W1^{i} bond. Therefore, there is a 50:50 distribution of two symmetry-related orientations of the Cp* ligand bonded to atom W2. In addition, the triflate anion is also located on a special position (another C_2 axis, orthogonally cutting through the C–S bond), yielding again a 50:50 distribution of two symmetry-related orientations. In spite of this problem, the structural model refined to quite acceptable final residuals, yielding relatively precise bond lengths and angles.

The crucial question concerns the absence of H atoms on the bridging O atoms. No residual electron density that could be assigned to such atoms was visible from the final difference Fourier map. However, even more convincing is the absence of close contacts between the two ions. The anion is located on the same plane as the W_3 triangle, separated from it by one of the Cp* ligands, see Figure 3. Two of the Cp* methyl H atoms are in close contact with the anion: H11B···O2 2.448, H11B···F11 2.506, H12C···O11 2.428, H12C···F12 2.540 Å. It may be reasonably argued that, if any OH group was present on the triangular W_3 cluster, this would establish H-bonding contacts with the triflate anion, as observed for the reduced analogue **1** (see above). Rather, the space above and below the W_3 triangle, in close contact with the bridging O atoms, is occupied by CH_3 groups of the $[Cp^*_3W_3O_6]^+$ ions located in other asymmetric units.

Two Trifluoroacetate Structures – Compounds 3 and 4

Before discussing the structural parameters within the $[Cp^*_3W_3O_6]^+$ ion in more detail, we introduce two additional compounds related to **2**. These were obtained from the same synthetic procedure shown above but by using CF_3COOH in place of triflic acid. Although the green product could not be obtained in single crystalline form, red crystals of the oxidation product were obtained after exposure to air. From two batches, crystallized under slightly different conditions, two different crystals containing the same $[Cp^*_3W_3O_6]^+$ ion were obtained: $[Cp^*_3W_3O_6][Zn_3(\mu_3\text{-}O)(\mu\text{-}CF_3COO)_4(CF_3COO)(CF_3COOH)(H_2O)_3]\cdot CF_3COOH$ (**3**) and $[Cp^*_3W_3O_6]_2[Zn(H_2O)_6](CF_3COO)_2(CF_3COOHOOCCF_3)_2\cdot 4H_2O$ (**4**). The bonding parameters for the tritungsten cluster of each compound are collected in Table 1, together with those of compounds **1** and **2**.

Compound **3** contains a complex, apparently unprecedented trinuclear zinc anion, as well as an interstitial CF_3COOH molecule as shown in Figure 4. The closest relatives appear to be $Zn_3(\mu_3\text{-}O)(\mu\text{-}CF_3COO)_x$ clusters with $x = 5$[15] or 6,[16] and with similar frameworks and geometries. The anion in compound **3** contains one four-coordinate (Zn2) and two six-coordinate (Zn1, Zn3) zinc ions joined together by a triply bridging ligand O4. One carboxylate ligand bridges atoms Zn1 and Zn2, a second one bridges atoms Zn2 and Zn3, two additional ones bridge atoms Zn2 and Zn3, and a fifth one is terminally bonded to the four-coordinate Zn2 atom. The latter one is disordered among two different positions, one of which features a H-bond to the aqua ligand identified by atom O2 [O71a···O2 = 2.70(2) Å]. The other position features two weaker H-bonding interactions, the first one with the same aqua ligand [O71···O2 = 3.11(3) Å] and the second one (not shown in Figure 4) with atom O92 of a coordinated acid ligand [O71···O92 = 3.02(2) Å]. The latter ligand is terminally bonded to atom Zn3 through the carbonyl oxygen atom O91, whereas the OH functionality of this ligand (O92) is engaged as a proton donor in H-bonding with the triply bridging oxygen atom O4. The most relevant H-bonding contacts in compound **3** are supplied in the Supporting Information. The coordination sphere of six-coordinate Zn1 is completed by two water molecules (O1 and O2), whereas that of six-coordinate Zn3 is completed by a third water molecule (O3). The interstitial acid is a proton donor to the OH group of the coordinated acid (O92) and an acceptor from one of the aqua ligands (O2). The anion also establishes H-bonding interactions, as a proton donor, with the W_3 cation: three stronger ones through the aqua ligands O1 and O3 (with atoms O21, O23, and O13^{i}), plus two weaker ones through the aqua ligands O3 (with atom O12^{i}) and O2 (with atom O22), see Figure 5. H-bonding interactions are established on both opposite sides of the triangular W_3 face, which results in zig–zag 1D H-bonded chains (see Figure S1, Supporting Information). The most significant bonding parameters of the $[Zn_3(\mu_3\text{-}O)(\mu\text{-}CF_3COO)_4(CF_3COO)(CF_3COOH)(H_2O)_3]^-$ anion are collected in Table 2.

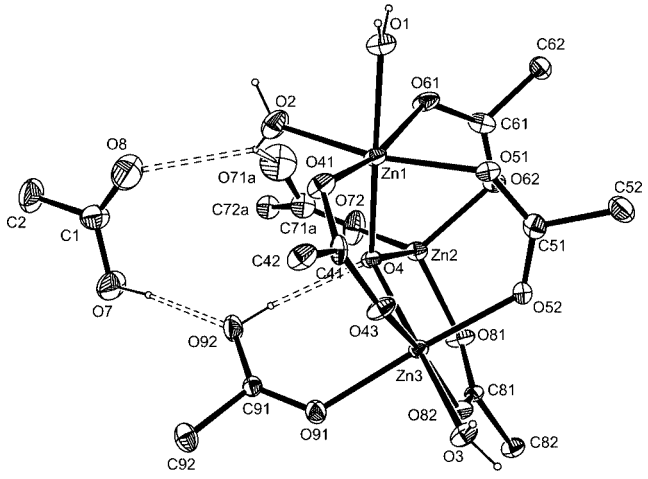

Figure 4. A view of the $[Zn_3(\mu_3\text{-}O)(\mu\text{-}CF_3COO)_4(CF_3COO)(CF_3COOH)(H_2O)_3]^-$ anion and the interstitial CF_3COOH molecule in compound **3**. Only one component (C71a, C72a, and O71a) of the disordered CF_3COO group is shown for the sake of clarity.

Compound **4** features a $[Zn(H_2O)_6]^{2+}$ ion sitting on an inversion center, plus an isolated CF_3COO^- ion, a homoconjugate $CF_3COO\cdots H\cdots OOCCF_3^-$ ion, and two water molecules in general positions, in addition to the $[Cp^*W_3O_6]^+$ ion, also located in a general position. The three bridging O atoms on one face of the W_3 triangle (O21, O22, and O23) are acceptors for H-bonds with the aqua ligands of the $[Zn(H_2O)_6]^{2+}$ cation, see Figure 6. The opposite face of the W_3 triangle (atoms O11, O12, and O13) does not establish H-bonds. In addition, the aqua ligands of the

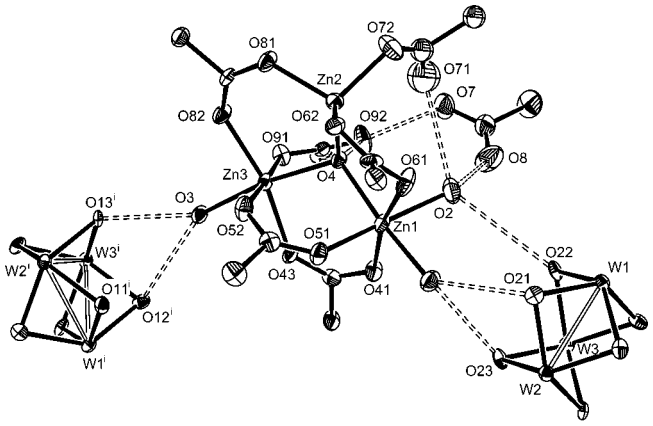

Figure 5. A view of the arrangement between the $[Zn_3(\mu_3\text{-}O)(\mu\text{-}CF_3COO)_4(CF_3COO)(CF_3COOH)(H_2O)_3]^-$ anion, the interstitial CF_3COOH molecule, and the $[Cp^*_3W_3O_6]^+$ cation in compound **3**. The cation Cp* ligands and the aqua H atoms have been removed and only the coordination spheres of the Zn atoms are shown for clarity [symmetry code: (i) 1/2 + *x*, 3/2 – *y*, *z* – 1/2].

Table 2. Relevant bond lengths and angles for the $[Zn_3(\mu_3\text{-}O)(\mu\text{-}CF_3COO)_4(CF_3COO)(CF_3COOH)(H_2O)_3]^-$ anion of compound **3**.

Bond lengths [Å]			
Zn1–O1	2.047(6)	Zn2–O81	1.966(7)
Zn1–O41	2.050(6)	Zn2–O62	1.970(6)
Zn1–O51	2.065(7)	Zn3–O3	2.068(6)
Zn1–O4	2.076(6)	Zn3–O52	2.070(6)
Zn1–O12	2.098(7)	Zn3–O4	2.092(6)
Zn1–O61	2.229(6)	Zn3–O82	2.108(6)
Zn2–O72	1.953(7)	Zn3–O91	2.122(6)
Zn2–O4	1.954(5)	Zn3–O43	2.132(6)
Bond angles [°]			
O4–Zn1–O1	172.8(2)	O4–Zn3–O31	170.9(2)
O4–Zn1–O2	91.6(3)	O4–Zn3–O43	94.4(2)
O4–Zn1–O41	99.5(2)	O4–Zn3–O52	90.6(2)
O4–Zn1–O51	93.4(2)	O4–Zn3–O82	100.6(2)
O4–Zn1–O61	93.7(2)	O4–Zn3–O91	92.0(2)
O1–Zn1–O2	85.7(3)	O3–Zn3–O43	76.6(2)
O1–Zn1–O41	87.3(3)	O3–Zn3–O52	89.0(3)
O1–Zn1–O51	88.0(3)	O3–Zn3–O82	88.4(2)
O1–Zn1–O61	79.4(3)	O3–Zn3–O91	88.8(3)
O2–Zn1–O41	92.8(3)	O43–Zn3–O52	94.5(3)
O2–Zn1–O51	168.1(3)	O43–Zn3–O82	164.8(3)
O2–Zn1–O61	84.7(3)	O43–Zn3–O91	87.2(3)
O41–Zn1–O51	97.0(3)	O52–Zn3–O82	87.7(3)
O41–Zn1–O61	166.7(3)	O52–Zn3–O91	176.8(3)
O51–Zn1–O61	84.2(3)	O82–Zn3–O91	89.9(3)
O4–Zn2–O62	112.7(2)	Zn1–O4–Zn2	111.2(3)
O4–Zn2–O72	115.0(3)	Zn1–O4–Zn3	112.1(2)
O4–Zn2–O81	112.3(3)	Zn2–O4–Zn3	111.0(3)
O62–Zn2–O72	107.4(3)		
O62–Zn2–O81	103.6(3)		
O72–Zn2–O81	105.0(3)		

$[Zn(H_2O)_6]^{2+}$ cation are H-bond donors towards the interstitial water molecules ($O111^i$ to O2W and $O113^i$ to O1W) and to the free CF_3COO^- ion (O112 to O51). The other O atom of the latter (O52) is a H-bond acceptor from O1W. The homoconjugate anion, $CF_3COOHOOCCF_3^-$, also establishes H-bonds as acceptor with both interstitial water molecules. The relevant H-bonding parameters are provided in the Supporting Information. The H-bonding network yields an arrangement of the structure in 2D layers (see Figure S2, Supporting Information).

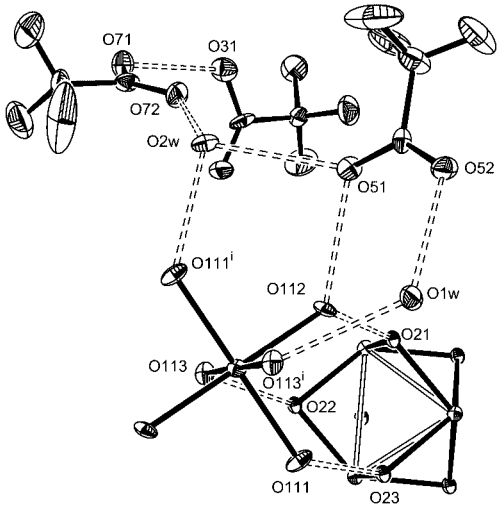

Figure 6. A view of the arrangement between the $[Cp^*_3W_3O_6]^+$, $[Zn(H_2O)_6]^{2+}$, CF_3COO^-, and $CF_3COO\cdots H\cdots OOCCF_3^-$ ions, and the two interstitial H_2O molecules, in the structure of compound **4**. The cation Cp* ligands and all H atoms have been removed for clarity [symmetry code: (i) –*x*, –*y*, –*z*].

Description of the $[Cp^*_3W_3O_6]^+$ Structure

The $[Cp^*_3W_3O_6]^+$ cluster has identical bonding parameters, within experimental error, in the structures of compounds **2**, **3**, and **4**, see Table 1. A representative view is shown in Figure 7. These parameters are significantly different from those of the dication of compound **1**. In particular, the three W–W distances are essentially equivalent, and they are placed in the narrow range 2.650–2.685 Å, with averages of 2.655(3) Å for **2**, 2.673(10) Å for **3**, and 2.662(2) Å for **4** or 2.663(10) Å for the entire set. This value is very close to the distance of the W–W bond bridged by

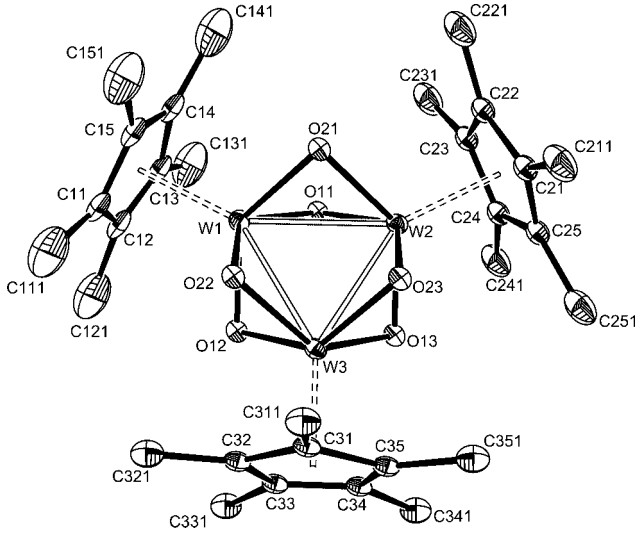

Figure 7. An ORTEP view of the $[Cp^*_3W_3O_6]^+$ ion from the structure of compound **3**.

two O ligands in compound **1**. The higher symmetry of the $Cp^*_3W_3O_6$ scaffold in the monocation, approaching ideal D_{3h} symmetry, is also revealed by the small spread of the W–O distances [range 1.918–1.998 Å; averages 1.960(10) Å for **2**, 1.964(16) Å for **3**, 1.948(17) Å for **4**; global average 1.957(16) Å] and W–O–W angles [range 84.9–87.5°; averages 85.2(4)° for **2**, 85.8(4)° for **3**, 86.2(8)° for **4**; global average 85.7(7)°]. These values are also close to those of the $W(\mu\text{-}O)_2W$ moiety in compound **1**.

Spectroscopic Identification

According to the formulation of the two clusters, derived from the X-ray analyses shown above, as $[Cp^*_3W_3O_4(OH)_2]^{2+}$ for the green derivative and $[Cp^*_3W_3O_6]^+$ for the red-orange derivatives, the first cluster has three metal electrons and should therefore be paramagnetic, whereas the second one has only two, which should be located in a symmetric metal–metal bonding combination,[13] and should therefore be diamagnetic. These expectations are in agreement with the experiment.

Compound **1** does not exhibit any strong ^1H NMR spectroscopic signal. In contrast, it has an EPR resonance, although this is clearly visible only at low temperatures (<200 K). The frozen glass spectrum in CH_2Cl_2 solution is shown in Figure 8. The overall shape is close to that expected for tetragonal symmetry, though a slight splitting of the perpendicular component is clearly visible. This is in nice agreement with the asymmetry of the bridge system, which introduces a slight perturbation to the threefold symmetry of the W_3 triangle as also indicated by the W–W distances. The perpendicular component does not have sufficient resolution to reveal the ^{183}W satellites. The parallel component, conversely, shows them quite clearly (see enlargement in Figure 8b). This feature was satisfactorily simulated as the sum of three Lorentzians, plus a quadratic function to account for the baseline drift. The satellites correspond to ca. 15% of the total intensity, in agreement with coupling of the unpaired electron with only one of the three cluster W atoms (theoretical values of 14.4, 24.7, and 31.6% are expected for coupling to 1, 2, or 3 equiv. W atoms, respectively). This observation will be fully rationalized on the basis of the computational results (vide infra).

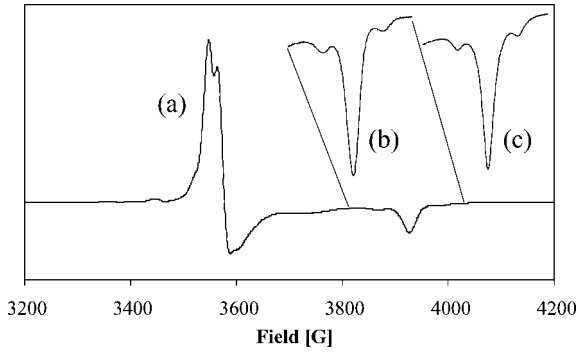

Figure 8. EPR spectrum of a frozen CH_2Cl_2 solution of compound **1** at 120 K: (a) experimental spectrum; (b) enlargement of the 3800–4050 G range; (c) simulation of (b), see text.

Contrary to compound **1**, compounds **2**–**4** do not show any EPR signal. They exhibit instead an NMR resonance at δ = 2.28 ppm in $CDCl_3$, consistent with the equivalence of the three Cp* ligands. Because this single ^1H NMR spectroscopic resonance is not conclusively proving the chemical constitution of the isolated bulk material, further characterization was sought by mass spectrometry (MS).

An electrospray ionization (ESI) MS study of compound **4** in CH_2Cl_2 gives a very clean isotopic cluster, which agrees with the theoretical isotopic distribution of $[Cp^*_3W_3O_6]^+$, see Figure 9. The same pattern is also observed in MeOH and in $MeOH/H_2O$ mixtures. Note the absence of fragmentation peaks, which reflects the robustness of the molecular

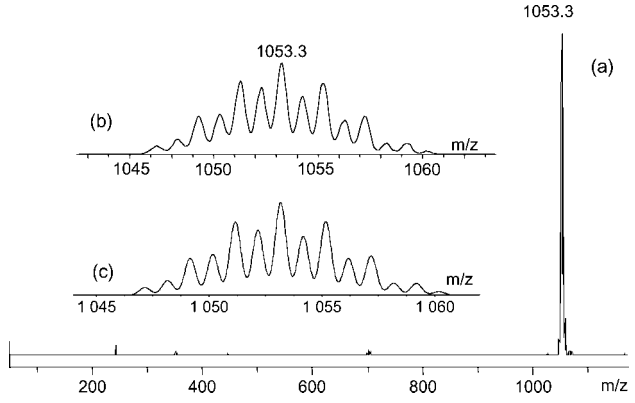

Figure 9. MS (ESI) of a CH_2Cl_2 solution of compound **4**. An expansion of the molecular ion isotopic cluster is shown in part (b) and the theoretical simulation in part (c).

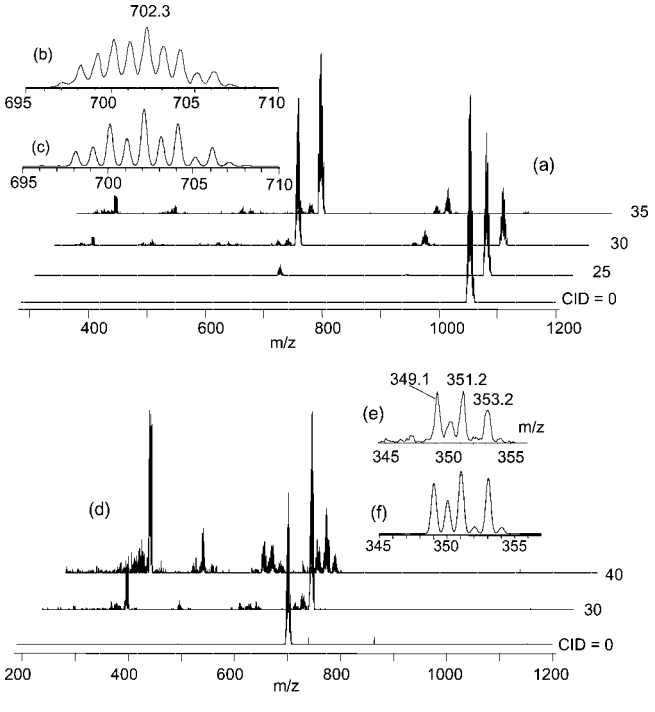

Figure 10. MS^n studies of the $[Cp^*_3W_3O_6]^+$ ion: (a) MS–MS(1053) at increasing collision energies; (b) expansion; and (c) simulation of the product ion; (d) MS–MS(1053)–MS(702) at increasing collision energies; (e) expansion; and (f) simulation of the product ion.

scaffold. To learn about the fragmentation pattern, the collision-induced decay (CID) of this ion was investigated by MS^n. As shown in Figure 10(a), the ion displays a major decay pathway by expulsion of a $[Cp^*WO_2]$ fragment with transformation into $[Cp^*_2W_2O_4]^+$ (isotope cluster centered at m/z = 702). However, the isotope pattern [Figure 10(b) with simulation in Figure 10(c)] reveals the presence of a second species one mass unit lighter. Therefore, elimination of a $[Cp^*WO_2H]$ unit, with the presumed involvement of a CH_3 group and generation of a tetramethylfulvene ligand, constitutes a competitive fragmentation pathway. Further trapping of these species and new CID in an MS^3 experiment, see Figure 10(d), is less selective but the major decay pathway is once again expulsion of a $[Cp^*WO_2]$ fragment from $[Cp^*_2W_2O_4]^+$, yielding $[Cp^*WO_2]^+$ (isotope cluster centered at m/z = 351). The latter ion is not produced in a major pathway by direct expulsion of $[Cp^*_2W_2O_4]$ from the trinuclear species.

DFT Calculations

Model compounds of the triangular W_3 clusters, obtained by replacing the Cp* ligands with the simpler Cp ring, i.e. $[Cp_3W_3O_4(OH)_2]^{2+}$ (**5**) for compound **1** and $[Cp_3W_3O_6]^+$ (**6**) for compounds **2**–**4**, were subjected to geometry optimization to find further supporting evidence for their stoichiometry (notably the number of OH vs. O groups) and to investigate their electronic structure. The calculations were run with no symmetry restrictions. Both calculations converged smoothly, giving final geometries in remarkably good agreement with the corresponding experimental ones for the Cp* derivatives (see Table 3). The only slight discrepancy consists of slightly longer bond lengths from the calculations relative to the experiment (W–O distances by 0.02–0.05 Å; W–W distances by 0.06–0.10 Å), as is typically observed for DFT calculations.

The geometrical trends for the less symmetric dihydroxido cluster **5** (see Scheme 1) are perfectly reproduced. Particularly notable is the difference between the W–W and W–W′ distances. The dioxido-bridged (W–W) bond is shorter than the two oxidohydroxido-bridged (W–W′) bonds by about 0.1 Å, like in the experimental structure. The lengths of different types of W–O bonds also have the same trend in the calculated and experimental structures (b > d > a > c, for the labeling, refer to Scheme 1), as do the different types of W–OH bonds (e > f). Finally, the two W–CG distances are longer than the W′–CG′ distance.

Excellent agreement is also found between the optimized geometry for the $[Cp_3W_3O_6]^+$ cluster and the experimentally observed structure for the Cp* analogue. In particular, the geometry is now close to the ideal D_{3h} symmetry, with three very similar W–W distances. Note that the average optimized W–W distance in **6** is essentially identical to the shorter W–W distance for the dioxido-bridged bond in **5**. The same phenomenon is observed in the experimental structures. The three W–CG distances are also essentially equivalent.

Table 3. Comparison of the DFT optimized geometries (distances [Å], angles [°]) for the model $[Cp_3W_3O_4(OH)_2]^{2+}$ (**5**) and $[Cp_3W_3O_6]^+$ (**6**) complexes with the X-ray structures of the Cp* analogues.[a]

Parameter[b,c]	$[(C_5R_5)_3W_3O_4(OH)_2]^{2+}$	
	R = H (DFT) (**5**)	R = Me (X-ray)[d]
W–W	2.723	2.6545(3)
W–W′	2.839, 2.853	2.745(6)
W–(μ-O) (a)	1.920, 1.914	1.902(4)
W–(μ-O) (b)	2.049, 2.054	2.005(4)
W–(μ-O) (c)	1.894, 1.896	1.877(5)
W′–(μ-O) (d)	2.012, 2.018	1.990(11)
W–(μ-OH) (e)	2.148, 2.152	2.078(4)
W′–(μ-OH) (f)	2.091, 2.091	2.042(7)
W–CG	2.096, 2.099	2.043(14)
W′–CG′	2.060	2.003(2)
W′–W–W′	57.17	57.829(7)
W–W′–W′	61.66, 61.17	61.08(13)
W–(μ-O)–W (a–b)	86.60, 86.60	85.54(14)
W–(μ-O)–W′ (c–d)	93.16, 93.60	90.40(15)
W–(μ-OH)–W′ (e–f)	84.09, 84.49	83.6(3)
CG-W–(μ–O) (a)	112.28, 113.29	112.5(4)
CG–W–(μ-O) (b)	113.86, 115.23	112.8(4)
CG–W–(μ-O) (c)	110.54, 111.46	111.4(3)
CG–W′–(μ-O) (d)	113.85, 115.97	114.1(12)
CG–W–(μ-OH) (e)	115.33, 116.00	113.9(7)
CG′–W′–(μ-OH) (f)	116.11, 116.37	114.7(12)
Parameter	$[(C_5R_5)_3W_3O_6]^+$	
	R = H (DFT) (**6**)	R = Me (X-ray)[e]
W–W	2.725, 2.732, 2.717	2.663(10)
W-(μ-O)	1.946, 2.014, 1.932, 2.038, 1.919, 2.047, 1.919, 2.054, 1.918, 2.047, 1.937, 2.037	1.957(16)
W–CG	2.108, 2.109, 2.110	2.053(7)
W–W–W	59.71, 60.01, 60.28	60.0(2)
W-(μ-O)–W	86.99, 85.95, 86.63, 87.03, 87.05, 86.24	85.7(7)
CG–W-(μ-O)	114.55, 113.05, 112.90, 114.23, 112.56, 114.42, 114.56, 112.92, 113.39, 114.48, 112.47, 113.93	113(1)

[a] The experimental parameters (X-ray structures) that are chemically and geometrically equivalent are averaged; for the individual parameters, see Table 1. [b] Label W refers to the two geometrically equivalent W atoms; W′ refers to the unique atom sitting on the ideal C_2 symmetry axis; CG and CG′ are the centers of gravity of the rings bonded to atoms W and W′, respectively. [c] For the labels assigned to geometrically different W–O and W–OH bonds (a–f), refer to Scheme 1. [d] From the structure of compound **1**. [e] Averaged values from the structures of compounds **2**–**4**.

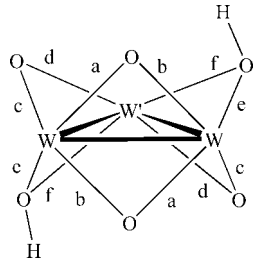

Scheme 1. Labeling of geometrically different W–O bonds in the structure of $[Cp_3W_3O_4(OH)_2]^{2+}$. The ideal C_2 symmetry axis passes through atom W′ and through the midpoint of the W–W vector. The Cp ligands are not drawn for the sake of clarity.

The electronic structure analysis is particularly interesting. The qualitative interaction diagram for the metal-based orbitals in this type of molecular scaffold was previously discussed[17,18] and is reproduced in Scheme 2 for convenience. The relevant metal-based molecular orbitals calculated for the two systems are shown in Figure 11, whereas more extensive data are available in the Supporting Information. For system **6** – a 2-electron $W_3^{V,V,VI}$ cluster – the two metal electrons are located in the $a(z^2)$ orbital, as expected. This orbital interaction insures the metal–metal attractive force. The additional electron in system **5** – a 3-electron $W_3^{V,V,V}$ cluster – is located in one of the two orbitals derived from the $e(xy)$ set. Because the ideal symmetry is reduced from D_{3h} to C_2 by the addition of the two protons, the $e(xy)$ set splits (e_1 of a type + e_2 of b type) and the unpaired electron is located in the symmetric a component. Note that, whereas the antisymmetric (b) component must be nil on the unique tungsten atom (W′) (see Supporting Information), there is no symmetry restriction for the composition of the a-type orbital. However, the composition of this orbital is such that the contribution from the two symmetry-equivalent W atoms is negligible, whereas atom W′ contributes greatly. Thus, the spin density is very much localized on the W′ atom (0.911), whereas it is negligible on the two W atoms (0.028 and 0.036), in perfect agreement with the measured relative intensity of the satellites in the EPR spectrum (vide supra). In this respect, it should be noted that the related molybdenum complex $[Cp^*_3Mo_3O_2(OH)_4]^{2+}$ – a 5-electron $Mo_3^{IV,IV,V}$ cluster – was shown to have the same ordering for the metal-based molecular orbitals.[13] Therefore, the unpaired electron for that complex is located in the antisymmetric b orbital and couples to only two Mo nuclei, again consistent with the experimental evidence from EPR spectroscopy.

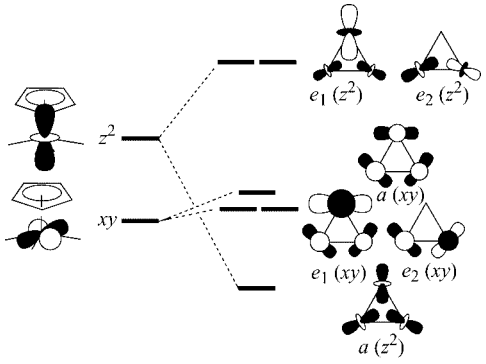

Scheme 2. Qualitative metal–metal orbital interactions for a $Cp_3M_3L_6$ molecule of ideal D_{3h} symmetry.

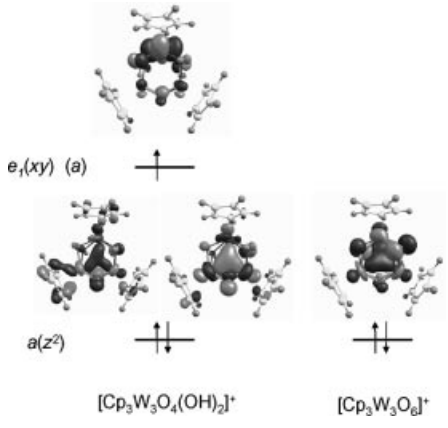

Figure 11. Filled metal-based molecular orbitals for systems **5** (left) and **6** (right). For the former, both spin orbitals resulting from the spin unrestricted calculation are shown.

Comparison with Molybdenum and Redox Considerations

The reduction process reported here parallels that reported recently for the reduction of $Cp^*_2Mo_2O_5$.[13] However, the Mo system leads to a deeper reduction with generation of a 5-electron cluster, the trinuclear $Mo_3^{IV,IV,V}$ $[Cp^*_3Mo_3O_2(OH)_4]^{2+}$ complex. This product has the same molecular architecture as the two trinuclear W clusters described here, differing only by the number of protons and electrons. This difference agrees with the general trend of greater stability for higher oxidation states upon descending the same group of transition metals. It may be predicted that, by treatment with suitable oxidizing agents (or at a suitable electrochemical potential in an electrochemical experiment) the 5-electron Mo cluster could produce a 3-electron or a 2-electron cluster with the same structure found in the present study for the W system. Conversely, suitable reductive treatment of the W system could afford a 5-electron system such as the previously reported Mo cluster. Other electronic configurations such as 4-electron $M^{IV,V,V}$ could also exist. Given that proton gains/losses are associated with these transformations (at least between the two types of W clusters reported in the present contribution), it may also be expected that the redox potential is pH dependent in a protic environment. A detailed analysis of the electrochemical behavior of these clusters is beyond the scope of the present investigation and may be carried out at a later time.

Previous studies of the $Cp^*_2Mo_2O_5$ system by a coupled electrochemical–electrospray mass spectrometry methodology, by using a flow-through electrochemical cell,[19,20] revealed a very rich redox behavior, including the formation of trinuclear clusters that are related to the isolated cluster. We have now attempted to carry out a similar investigation for $Cp^*_2W_2O_5$, but no sufficient quantities of soluble products were revealed by the mass spectrometric analysis. At the potential at which the Mo system started to yield reductive processes, the W system showed no activity, whereas the rapid formation of a film on the surface of the electrode, which blocked any further electrochemical transformation, was observed at lower potentials. Therefore, it seems that the $Cp^*_2W_2O_5$ is more difficult to reduce than the Mo analogue and the primary reduction products (perhaps including the isolated trinuclear clusters described here) are unstable under these highly reducing conditions and proceed further to yield insoluble products.

Conclusions

Like its Mo analogue,[13] the compound $[Cp^*_2W_2O_5]$ can be reduced in an aqueous medium to a triangular metal–metal bonded cluster. However, only 2- and 3-electron clusters are obtained for W, whereas the Mo system undergoes a deeper reduction to yield a 5-electron cluster. Like for the Mo cluster, the oxido/hydroxido asymmetry in the bridge system splits the degeneracy of the "*e*"-type frontier orbitals, as indicated by the EPR spectrum of the 3-electron cluster and confirmed by the DFT calculations. The variability of the cluster electrons for this system will be further explored for applications in organometallic chemistry and catalysis.

Experimental Section

General Procedures: All preparations and manipulations were carried out with Schlenk techniques under an oxygen-free argon atmosphere. All glassware was oven-dried at 120 °C. Solvents were dried by standard procedures and distilled under nitrogen prior to use. ^{1}H NMR spectra were recorded with a Bruker AM 250. Chemical shifts are expressed in ppm downfield from Me_4Si. Coupling constants are given in Hertz. Mass spectra were recorded with a Finnigan (San Francisco, USA) LCQ quadrupole ion-trap mass spectrometer equipped with an electrospray-ionization (ESI) interface. The ESI was operated in the positive ion mode with a spray voltage of 4.5 kV. The capillary voltage was 20 V and the source temperature was 100 °C. Mass spectra were obtained by scanning the mass analyzer from *m*/*z* 100 to 2000 with 5 total microscans. Maximum inject time was 400 ms. The analyzer was operated at a background pressure of 2×10^{-5} Torr. In all experiments, helium was introduced at an estimated pressure of 1 mTorr to improve the ion-trapping efficiency and as collision gas for the collision-induced dissociation events. The compounds were isolated in the ion trap with an isolation width of 12 *m*/*z* units and activated by using increased collision energy to obtain collision-energy-dissociation profiles. EPR measurements were carried out at the X-band microwave frequency with a Bruker ESP300 spectrometer. The spectrometer frequency was calibrated with diphenylpicrylhydrazyl (DPPH, $g = 2.0037$). The starting compound, $[Cp^*_2W_2O_5]$, was prepared as described in the literature.[14]

Synthesis and Crystallization of $[Cp^*_3W_3O_4(OH)_2](CF_3SO_3)_2 \cdot 2H_2O$ (1): Metallic zinc (20 mesh, 0.415 g, 6.34 mmol) was added to a solution of $[Cp^*_2W_2O_5]$ (50 mg, 0.070 mmol) in MeOH/H_2O (1:1, 6 mL). The mixture was acidified with CF_3SO_3H (10 drops) and stirred under an atmosphere of argon at r.t. for 3 d, during which time it changed from a yellow solution to a green suspension. The mixture was filtered, and the solid was extracted with THF (0.5 mL). The addition of Et_2O (1.5 mL) to the filtrate yielded the product as a green precipitate (0.047 g, 72%). A single crystal for X-ray analysis was obtained by diffusion of an Et_2O layer into a THF solution at r.t. EPR (X-band, CH_2Cl_2, 120 K): $g_\perp = 1.89$; $g_\parallel = 1.72$ ($a_{W\parallel} = 114$ G).

Synthesis and Crystallization of $[Cp^*_3W_3O_6](CF_3SO_3)$ (2): A sample of compound **1** (61 mg, 0.044 mmol) was dissolved in CH_2Cl_2 and stirred for 1 h at r.t. in open air. The color of the green solution turned orange. The solvent was evaporated to dryness to afford an orange power, which was recrystallized from CH_2Cl_2/pentane to give red crystals (25 mg, 47% yield). ^{1}H NMR (250 MHz, $CDCl_3$): $\delta = 2.28$ ppm.

Reduction of $[Cp^*_2W_2O_5]$ by Zinc in the Presence of CF_3COOH – Formation of Compounds 3 and 4: Metallic zinc (20 mesh, 0.415 g, 6.34 mmol) was added to a solution of $[Cp^*_2W_2O_5]$ (50 mg, 0.070 mmol) in MeOH/H_2O (1:1, 6 mL). The mixture was acidified with CF_3COOH (10 drops) and stirred under an atmosphere of argon at r.t. for 5 d during which time it changed from a yellow solution to a green suspension. The mixture was filtered, and the solid was dried under vacuum (31 mg). Attempts to produce single crystals from this material failed as only powdery precipitates were obtained. Red single crystals of compound **3** were eventually obtained from CH_2Cl_2/hexane after exposure of the solution to air. ^{1}H NMR (250 MHz, CD_2Cl_2): $\delta = 2.26$ ppm.

In a parallel identical procedure, from one of the numerous attempts to crystallize the green solid, the yellow mother solution of the green powdery precipitate was recovered, dried, and the yellow-orange residue was set again for crystallization from THF/hexane to yield single crystals of compound **4**. ^{1}H NMR (250 MHz, $CDCl_3$): $\delta = 2.28$ ppm. MS (ESI, CH_2Cl_2): $m/z = 1053$ (envelope) $[M]^+$ (see Results and Discussion section).

X-Ray Diffraction Studies: A single crystal of each compound was mounted under inert perfluoropolyether at the tip of a glass fiber and cooled in the cryostream of an Oxford-Diffraction XCALIBUR CCD diffractometer. Data were collected by using the monochromatic MoK_α radiation ($\lambda = 0.71073$). The structures were solved by direct methods (SIR97)[21] and refined by least-squares procedures on F^2 by using SHELXL-97.[22] All H atoms attached to carbon were introduced at idealized positions and treated with the riding model. All H atoms attached to oxygen were either located on difference Fourier syntheses or their coordinates were calculated on the basis of hydrogen bonding geometry and energy considerations.[23] They were then treated as riding on their parent O atoms. In compound $Cp^*_3W_3O_6(CF_3SO_3)$, the cation, $Cp^*_3W_3O_6$, is arranged around a twofold axis resulting in one of the Cp* to be disordered over two positions. The CF_3SO_3 anion is also disordered and arranged around another twofold axis. For both the disordered parts, the atomic positions and anisotropic thermal parameters were restrained to reasonable values using the tools available within SHELXL-97.[22] The drawing of the molecules was realized with the help of ORTEP3.[24] Crystal data and refinement parameters are shown in Table 4. CCDC-643997 to -644000 contain the supplementary crystallographic data for this paper. These data can be obtained free of charge from the Cambridge Crystallographic Data Centre via www.ccdc.cam.ac.uk/data_request/cif.

Computational Details: The DFT calculations were carried out on model systems where the Cp* ligands were replaced on the simpler Cp rings. The starting geometries were based on the crystallographically determined structures and no symmetry restrictions were imposed. The geometries were fully optimized and the resulting minima of the potential energy surface (PES) were verified by the positive value of all second derivatives of the energy. The calculations were performed by using the B3LYP three-parameter hybrid density functional method of Becke[25] and the standard LANL2DZ basis set, which included the Hay and Wadt effective core potentials (ECP) for the tungsten atoms,[26] as implemented in the Gaussian03 suite of programs.[27] The calculation on the open-shell system **5** was carried out by using the spin-unrestricted formulation. The value of $<S^2>$ resulting from the calculation is 0.7575, indicating negligible spin contamination.

Supporting Information (see footnote on the first page of this article): Packing diagrams for compounds **3** and **4**, energy diagrams

Table 4. Selected crystallographic and refinement parameters for all compounds.

Compound	**1**	**2**	**3**	**4**
Empirical formula	$C_{32}H_{49}F_6O_{14}S_2W_3$	$C_{31}H_{45}F_3O_9SW_3$	$C_{44}H_{53}F_{21}O_{24}W_3Zn_3$	$C_{36}H_{53}F_9O_{17}W_3Zn_{0.5}$
Formula weight	1387.38	1202.28	2112.52	1513.02
Temperature [K]	180(2)	180(2)	180(2)	180(2)
Wavelength [Å]	0.71073	0.71073	0.71073	0.71073
Crystal system	monoclinic	monoclinic	monoclinic	triclinic
Space group	$P2_1/a$	$C2/c$	Cc	$P\bar{1}$
a [Å]	19.6490(7)	16.7981(11)	12.9884(12)	12.8993(12)
b [Å]	11.1968(4)	15.1424(7)	21.8922(15)	13.2879(13) Å
c [Å]	19.7744(8)	14.9343(8)	22.862(2)	16.6848(18) Å
α [°]	90	90	90	96.016(8)
β [°]	106.433(3)	113.172(5)	90.493(7)	104.993(9)
γ [°]	90	90	90	116.737(9)
Volume [Å^3]	4172.8(3)	3492.3(3)	6500.5(9)	2384.7(4)
Z	4	4	4	2
Density (calculated) [mg m^{-3}]	2.208	2.287	2.159	2.107
Absorption coefficient [mm^{-1}]	8.438	9.984	6.509	7.564
F(000)	2644	2272	4040	1446
Crystal size [mm]	0.27 × 0.14 × 0.09	0.26 × 0.205 × 0.043	0.32 × 0.2 × 0.126	0.34 × 0.15 × 0.034
θ range [°]	2.79 to 26.37	3.65 to 30.03	3.20 to 28.28	2.61 to 25.03
h, k, l ranges	–24 to 24	–23 to 16	–16 to 17	–15 to 15
	–13 to 13	–21 to 21	–29 to 29	–15 to 14
	–23 to 24	–19 to 21	–30 to 29	–19 to 18
Reflections collected	29412	17199	28767	14697
Independent reflections	8524 [R(int) = 0.0348]	5088 [R(int) = 0.0369]	11663 [R(int) = 0.0547]	8107 [R(int) = 0.0691]
Completeness to θ = 25.00° [%]	99.8	99.7	99.9	96.3
Absorption correction	multi-scan	multi-scan	multi-scan	multi-scan
Max. and min. transmission	0.3589 and 0.1896	0.3236 and 0.1509	1.0 and 0.2368	
Refinement method	full-matr. least-sq. (F^2)	full-matr. least-sq. (F^2)	full-matr. least-sq. (F^2)	full-matr. least-sq. (F^2)
Data/restraints/parameters	8524/8/547	5088/32/226	11663/32/857	8107/0/436
Goodness-of-fit on F^2	1.124	1.182	0.923	0.867
$R1$, $wR2$ [$I > 2\sigma(I)$]	0.0324, 0.0738	0.0417, 0.0883	0.0382, 0.0619	0.0502, 0.0921
$R1$, $wR2$ (all data)	0.0413, 0.0772	0.0484, 0.0909	0.0502, 0.0649	0.1356, 0.1097
Absolute structure parameter			0.007(6)	
Largest diff. peak and hole [e Å^{-3}]	3.747 and –1.748	2.455 and –3.030	1.489 and –1.302	4.859 and –1.751

and representative molecular orbitals for systems **5** and **6** (5 pages), H-bonding parameters of **1**, **3**, and **4**.

Acknowledgments

We are grateful to the European Commission for funding of this work through the AQUACHEM Research Training Network (Project no. MRTN-CT-2003-503864). We also thank CINES and CICT (project CALMIP) for a grant of free computer time. Supplemental travel support was provided by a Bosphorus bilateral Program of Integrated Actions, co-sponsored by the French Ministry of Foreign Affairs in France and by TUBITAK in Turkey [TBAG-U/142(105T256)].

[1] T. Chan, L. Li, Y. Yang, W. Lu, *ACS Symp. Ser.* **2002**, *819*, 166–177.
[2] F. Joó, *Acc. Chem. Res.* **2002**, *35*, 738–745.
[3] I. T. Horvath, *Acc. Chem. Res.* **2002**, *35*, 685.
[4] D. Sinou, *Top. Curr. Chem.* **1999**, *206*, 41–59.
[5] D. Sinou, *Adv. Synth. Catal.* **2002**, *344*, 221–237.
[6] G. E. Jaouen, *J. Organomet. Chem.* **1999**, *589* (special issue: bioorganometallic chemistry).
[7] P. Kalck, F. Monteil, *Adv. Organomet. Chem.* **1992**, *34*, 219–284.
[8] B. E. Hanson, *Coord. Chem. Rev.* **1999**, *186*, 795–807.
[9] C. Muller, D. Vos, P. Jutzi, *J. Organomet. Chem.* **2000**, *600*, 127–143.
[10] A. Bino, F. A. Cotton, Z. Dori, *J. Am. Chem. Soc.* **1981**, *103*, 243–244.
[11] A. Bino, M. Ardon, E. Shirman, *Science* **2005**, *308*, 234–235.
[12] R. Poli, *Chem. Eur. J.* **2004**, *10*, 332–341.
[13] F. Demirhan, B. Çagatay, D. Demir, M. Baya, J.-C. Daran, R. Poli, *Eur. J. Inorg. Chem.* **2006**, 757–764.
[14] C. Dinoi, G. Taban, P. Sözen, F. Demirhan, J.-C. Daran, R. Poli, *J. Organomet. Chem.* **2007**, *692*, 3743–3749.
[15] A. L. Grzesiak, F. J. Uribe, N. W. Ockwig, O. M. Yaghi, A. J. Matzger, *Angew. Chem. Int. Ed.* **2006**, *45*, 2553–2556.
[16] J. S. Seo, D. Whang, H. Lee, S. I. Jun, J. Oh, Y. J. Jeon, K. Kim, *Nature* **2000**, *404*, 982–986.
[17] P. Kubácek, R. Hoffmann, Z. Havlas, *Organometallics* **1982**, *1*, 180–188.
[18] T. A. Albright, J. K. Burdett, M. H. Whangbo, *Orbital Interactions in Chemistry*, John Wiley & Sons, New York, **1985**.
[19] J. Gun, A. Modestov, O. Lev, D. Saurenz, M. A. Vorotyntsev, R. Poli, *Eur. J. Inorg. Chem.* **2003**, 482–492.
[20] J. Gun, A. Modestov, O. Lev, R. Poli, *Eur. J. Inorg. Chem.* **2003**, 2264–2272.
[21] A. Altomare, M. Burla, M. Camalli, G. Cascarano, C. Giacovazzo, A. Guagliardi, A. Moliterni, G. Polidori, R. Spagna, *J. Appl. Crystallogr.* **1999**, *32*, 115–119.
[22] G. M. Sheldrick, *SHELXL97: Program for Crystal Structure Refinement*, University of Göttingen, Göttingen, Germany, **1997**.
[23] M. Nardelli, *J. Appl. Crystallogr.* **1999**, *32*, 563–571.
[24] L. J. Farrugia, *J. Appl. Crystallogr.* **1997**, *32*, 565.
[25] A. D. Becke, *J. Chem. Phys.* **1993**, *98*, 5648–5652.
[26] P. J. Hay, W. R. Wadt, *J. Chem. Phys.* **1985**, *82*, 270–283.

[27] M. J. Frisch, G. W. Trucks, H. B. Schlegel, G. E. Scuseria, M. A. Robb, J. R. Cheeseman, J. Montgomery, J. A., T. Vreven, K. N. Kudin, J. C. Burant, J. M. Millam, S. S. Iyengar, J. Tomasi, V. Barone, B. Mennucci, M. Cossi, G. Scalmani, N. Rega, G. A. Petersson, H. Nakatsuji, M. Hada, M. Ehara, K. Toyota, R. Fukuda, J. Hasegawa, M. Ishida, T. Nakajima, Y. Honda, O. Kitao, H. Nakai, M. Klene, X. Li, J. E. Knox, H. P. Hratchian, J. B. Cross, C. Adamo, J. Jaramillo, R. Gomperts, R. E. Stratmann, O. Yazyev, A. J. Austin, R. Cammi, C. Pomelli, J. W. Ochterski, P. Y. Ayala, K. Morokuma, G. A. Voth, P. Salvador, J. J. Dannenberg, V. G. Zakrzewski, S. Dapprich, A. D. Daniels, M. C. Strain, O. Farkas, D. K. Malick, A. D. Rabuck, K. Raghavachari, J. B. Foresman, J. V. Ortiz, Q. Cui, A. G. Baboul, S. Clifford, J. Cioslowski, B. B. Stefanov, G. Liu, A. Liashenko, P. Piskorz, I. Komaromi, R. L. Martin, D. J. Fox, T. Keith, M. A. Al-Laham, C. Y. Peng, A. Nanayakkara, M. Challacombe, P. M. W. Gill, B. Johnson, W. Chen, M. W. Wong, C. Gonzalez, J. A. Pople, *Gaussian 03, Revision B.04*, Gaussian, Inc., Pittsburgh PA, **2003**.

Received: April 17, 2007
Published Online: July 24, 2007

